Seismic response of braced frames with and without friction dampers

Piero Colajanni and Maurizio Papia

Dipartimento di Ingegneria Strutturale e Geotecnica, Università di Palermo, Italy

(Received June 1993; revised version accepted December 1993)

The dynamic response of friction damped bracing systems and ordinary cross-bracing systems inserted into surrounding frames without lateral stiffness is analysed in order to compare the typical behaviour of the two different bracing systems. The cyclic force–displacement relationship in the two cases is accurately modelled on the basis of experimental and related numerical models which are available in the literature, and the structural dimensionless parameters defining the shapes of the cycles are stressed. Systems having the same average period of vibration in the elastic phase of the response are assumed to be comparable with one another, which leads to a relationship linking the structural parameters of the two kinds of system. Extending the ductility concept to the friction devices, by a step-by-step integration of the equation of motion for the two systems the dimensionless structural responses are derived with variations in the strength level factor. Computing the average values of the maximum responses to five accelerograms artificially generated to be compatible with the normalized elastic spectrum proposed by Eurocode 8, the behaviour factor versus period curves are also deduced with variations in the available ductility. These curves show the different reliability levels provided by the two kinds of bracing systems considered and they are useful for practical applications. Two meaningful numerical examples, carried out by assuming an input accelerogram corresponding to an actual seismic record (El Centro earthquake, 1940) confirm these design suggestions.

Keywords: earthquake engineering, seismic design, friction devices, bracing systems

The safety conditions of buildings in seismic regions depend greatly on the elastic characteristics of the structure and on its capacity to undergo strong earthquakes with moderate inelastic oscillations. Using design criteria based on the energy absorption concept, in the last few years a new approach, which is also useful for the seismic retrofitting of existing structures, has been proposed. It is based on the use of dissipative devices avoiding or minimizing plastic deformations of the main structural frame elements[1–11]. The seismic energy is dissipated by plastic deformation of special elements designed to this aim, or by slippage of the friction joints.

In this field the friction damping device proposed by Pall and Marsh[1] has been the object of several studies in order to: firstly, deduce a numerical model able to predict the cyclic experimental behaviour[5]; secondly, determine the optimum slip load minimizing structural damage[1,3,9]; thirdly, propose a criterion of distribution of the slip load along the height of friction damped multistorey structures[4,11]; and finally, compare the seismic response of frames with assigned geometrical and mechanical properties, stiffened by friction damping systems and concentric bracing systems[1,3,11]. The studies mentioned above provide much information about the performances of the dissipative system examined, but the design criteria which can be deduced cannot easily be generalized, because the results are often influenced by the stiffness and strength of the frame into which the bracing system is inserted. Moreover, the analysis of the behaviour of the friction damped bracing system (FDBS) and of the cross-bracing system (CBS) is carried out without specification of the structural parameters which make the two different systems comparable with one another.

On the basis of these remarks, this paper presents a parametric characterization of the seismic response of the FDBS and the CBS, analysing the behaviour of structures obtained

0141-0296/95/010129–12

by inserting the bracing systems to be examined into surrounding frames without lateral stiffness, made of axially inextensible elements with hinged joints. The results confirm the correctness of the provisions of several codes for the CBS, and show the field of practical use in which the FDBS proves to be advantageous in reducing design seismic forces.

Cyclic behaviour of friction damped bracing systems

The friction damping device scheme[1] and its location in the surrounding frame considered are shown in *Figures 1(a)* and *1(b)*, respectively. The device consists of four hinged links arranged to form a quadrilateral shape, and of two diagonal links also hinged at the joints of the horizontal and vertical links and arranged to be connected to external diagonal braces. Inside the quadrilateral region each of the diagonal links is made up of two separate parts which are partially superimposed by means of a friction brake joint located at the centre of the device.

For very low values of the horizontal force F acting on the rigid beam of the frame as in *Figure 1(b)*, the diagonal braces behave elastically and both confer lateral stiffness on the system. When F increases, the braces in compression reach the critical buckling load P_{cr}, while the braces in tension remain elastic; at this stage the system behaves like an ordinary cross-braced frame in the serviceable state. With further increases in F, the external buckled braces remain subjected to the critical load and the diagonal link in tension reaches the local slip load P_l at which the tension friction joint begins to slip; consequently, the load transmitted to the diagonal link in compression increases, until the local slip load P_l is also reached in the compression friction joint. The load distribution in the friction device, corresponding to the latter condition, is shown in *Figure 2*.

The load acting on the braces in tension reaches the maximum value

$$P_s = 2P_l - P_{cr} \qquad (1)$$

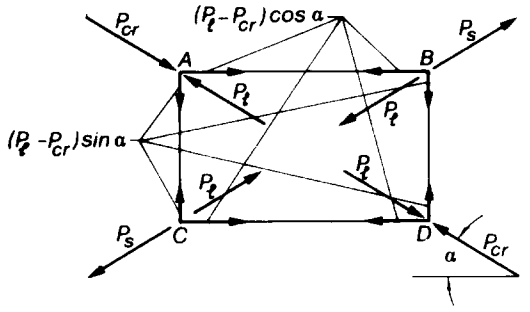

Figure 2 Distribution of forces at slippage phase of both joints

which is denoted as the global slip load. Further horizontal displacements of the rigid beam of the frame do not produce load variation in the elements of the system, which now does not have lateral stiffness. When the displacement of the rigid beam is reversed, the unloading phase begins. In this phase the simplifying assumption of instantaneous straightening of the buckled braces due to joint slippage can be made, or a rate of reversal displacement can be considered to be necessary to this occurrence. Filiatrault and Cherry[3] showed the latter to be a more realistic assumption. Therefore, the unloading curve of the force–displacement diagram of the friction damped frame can be obtained by translating the loading curve described above, starting from the maximum displacement value which was reached.

Considering the different behaviour phases in a loading and unloading cycle, one can conclude that the FDBS, with respect to the CBS, gives the double advantage of: firstly, preventing yielding of the tension braces, which produces deterioration of the hysteresis cycles, providing instead stable hysteretic slipping cycles; and secondly, rapidly restoring the straightened shape of the buckled braces, with consequent increase in the energy dissipated during the cycles following the first one.

The cyclic behaviour during a generic phase of motion of the frame in *Figure 1(b)*, subjected to a base excitation,

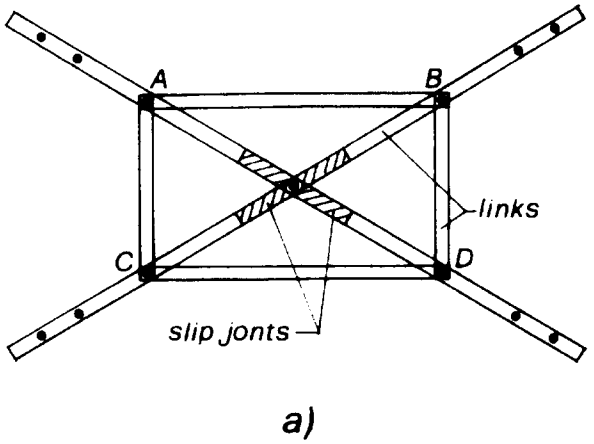

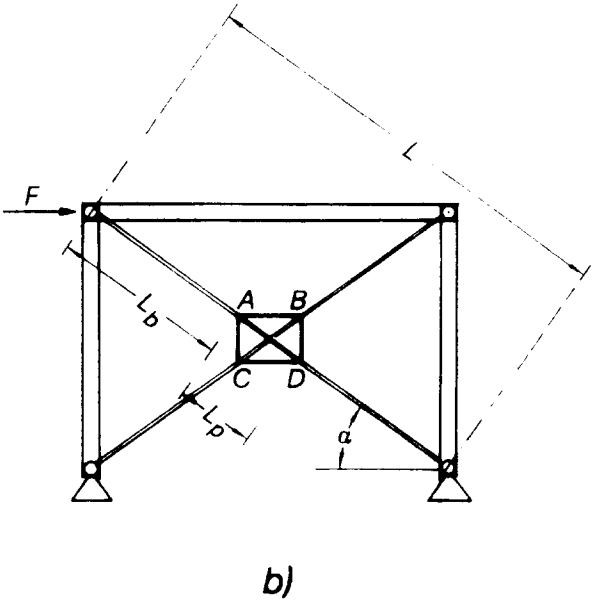

Figure 1 Friction damping system. (a) device scheme: (b) location in braced frame

is shown in *Figure 3* which shows the response phases described above. Assuming the links to have the same cross-sectional area A_d as the external braces, as in Reference 5, and considering the geometrical quantities shown in *Figure 1(b)*, the following parameters can be introduced

$$\gamma = 1 + 2(\cos^3\alpha + \sin^3\alpha) \quad \beta = \frac{\gamma + 1}{\gamma} \tag{2a}$$

$$l_b = \frac{L_b}{L} \qquad l_p = \frac{L_p}{L} \tag{2b}$$

$$l_1 = 2\beta l_b + l_p \qquad l_2 = (2 - \beta)(2l_b + \gamma l_p) \tag{2c}$$

Moreover, the displacements characterizing the cycle[5] can be expressed by

$$\Delta_1 = \frac{P_{cr}}{k_{o,d}} \cos\alpha \tag{3a}$$

$$\Delta_2 = \frac{P_l - P_{cr}}{k_{o,d}} l_1 \cos\alpha \tag{3b}$$

$$\Delta_3 = \frac{P_l - P_{cr}}{k_{o,d}} l_2 \cos\alpha \tag{3c}$$

where, denoting as E the modulus of elasticity

$$k_{o,d} = \frac{EA_d}{L} \cos^2\alpha \tag{4}$$

is the lateral stiffness contribution to the frame by a one-diagonal bracing system. In *Figure 3* Δs_1 and Δs_2 indicate the displacements produced by the slippages of the device during the cycle being examined; δ_0 is the residual horizontal displacement of the rigid beam due to the slippages of the device during the previous cycles. The shaded region shows the amount of dissipated energy which would be overestimated during a half-cycle considering for each buckled brace the simplified assumption of instantaneous straightening. Considering the load distribution in *Figure 2* and equation (1), the maximum ordinate of the force-displacement diagram in *Figure 3* is

$$F_{u,d} = 2P_l \cos\alpha \tag{5}$$

In each of the four different branches characterizing the cycle, which are numbered in *Figure 3*, the lateral stiffness of the system proves to be

$$k_{i,d} = k_{o,d} \frac{1}{c_{1i} l_b + c_{2i} l_p} \quad (1 \le i \le 4) \tag{6}$$

where the following values of the coefficients c_{1i}, c_{2i} are applicable: $c_{11} = 1$, $c_{12} = c_{13} = 2$, $c_{21} = 0.5$, $c_{22} = 1/\beta$, $c_{23} = \gamma$, and $c_{14} = c_{24} = \infty$.

Therefore, the force–displacement relationship for the frame in *Figure 1(b)* can be written in the form

$$F_{i,d} = k_{i,d}(\delta - \delta_o^*) + F_{oi,d} \quad (1 \le i \le 4) \tag{7}$$

where, with reference to the letters in *Figure 3*,

$$\delta_o^* = \begin{cases} \delta_o & \text{in the loading branches from A to B} \\ \delta_o + \Delta s_1 & \text{in the unloading branches from C to E} \\ \delta_o + \Delta s_1 - \Delta s_2 & \text{in the reloading branches from F to G} \end{cases} \tag{8}$$

and

$$F_{oi,d} = \pm \sum_{j=1}^{i} (k_{j,d} - k_{i,d}) \Delta_j \quad (1 \le i \le 4) \tag{9}$$

in which the sign must be assumed to be positive for the semicycle from A to D and negative for the semicycle from D to G.

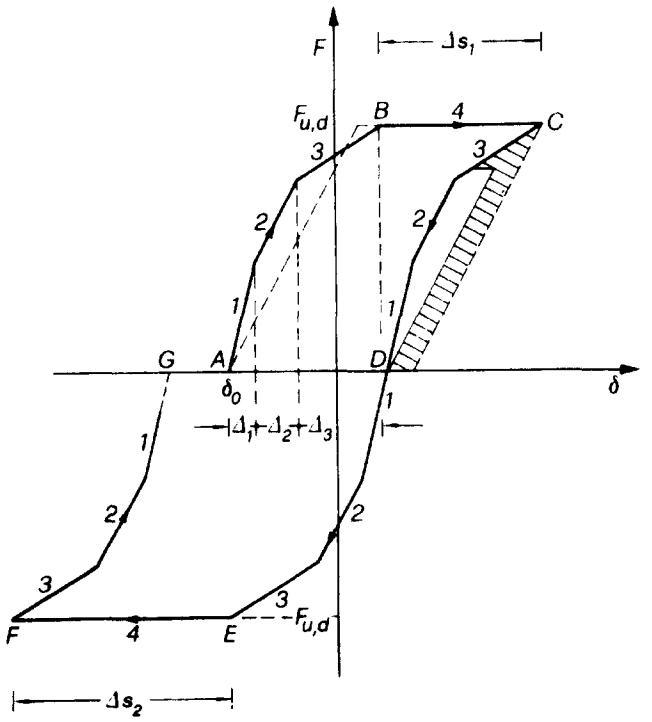

Figure 3 Force–displacement cycle for FDBS

Cyclic behaviour of cross-bracing systems

The cyclic behaviour of cross-braced frames has been theoretically and experimentally investigated[12–14]. During the first loading phase, the compression brace, which usually has high slenderness, buckles, undergoing large out-of-plane deflections. So, in the unloading phase, the system exhibits a noticeable loss of stiffness before the compression brace recovers the straightened shape. Moreover, a deterioration of the hysteresis cycles following the first one occurs, because of the simultaneous presence of tensile plastic deformations and flexural deformations due to buckling.

In the numerical analyses presented here, the cyclic behaviour of a single diagonal brace is modelled in agreement with the experimental results deduced by Ballio and Campanini[12]. The model adopted is also very similar to the one proposed by Maison and Popov[14]. The typical shape of the cyclic stress–strain relationship is shown in normalized

dimensionless form in *Figure 4*, where f and f_y are the brace generic stress and the yielding stress, respectively; $\epsilon = \Delta L/L$ is the variation ΔL in the brace length, measured in the plane of the frame in which the bracing system is inserted, divided by the initial length L; $\Delta\epsilon_{cr} = f_{cr}/E$ is the strain corresponding to the buckling critical stress; $\bar{\epsilon}_o = \epsilon_o/\Delta\epsilon_{cr}$ is the residual relative variation of length produced in the previous cycles normalized with respect to $\Delta\epsilon_{cr}$, and

$$\psi_c = \frac{f_{cr}}{f_y} \leq 1 \tag{10}$$

The diagram is characterized by the following quantities: $\Delta\bar{\epsilon}_2$ and α_1, depending on the slenderness of the diagonal brace; $\Delta\bar{\epsilon}_5$, which can be related to $\Delta\bar{\epsilon}_2$ by the equation $\Delta\bar{\epsilon}_5 = 0.2\Delta\bar{\epsilon}_2$; the angle α_2, depending on the slenderness of the brace and on the value $\Delta\bar{\epsilon}_{r1}$ from which the unloading phase begins; also the factor c which depends on the section shape of the brace.

Considering each of the eight branches of the curve numbered in *Figure 4*, the force–displacement relationship can be derived, as for the FDBS, in the form

$$F_{i,c} = k_{i,c}(\delta - \delta_o) + F_{oi,c} \quad (1 \leq i \leq 8) \tag{11}$$

where, with reference to the cycle in *Figure 4*, $\delta = \epsilon L/\cos\alpha$ and $\delta_o = \epsilon_o L/\cos\alpha$, while $k_{i,c}$ and $F_{oi,c}$ for each branch can be deduced from the dimensionless quantities indicated in *Table 1*.

In this table, the symbols α and L can be identified from *Figure 1(b)*; the initial lateral stiffness provided by the diagonal brace

$$k_{o,c} = \frac{EA_c}{L}\cos^2\alpha \tag{12}$$

is defined in the same way as in equation (4), A_c being the cross-sectional area of the brace; the normalized excursions $\Delta\bar{\epsilon}_{r1}$ and $\Delta\bar{\epsilon}_{r2}$, corresponding to the loading and unloading phases, respectively, are deducible from *Figure 4*, and

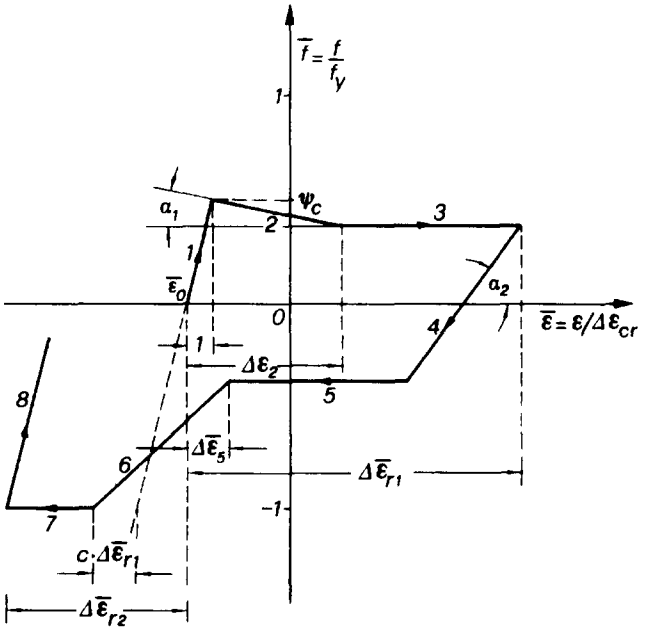

Figure 4 Normalized stress-strain cycle for single brace of CBS

$$\delta_y = \frac{f_y L}{E\cos\alpha} \tag{13}$$

is the horizontal displacement of the rigid beam producing the first yielding of the tension brace.

The force–displacement relationship for a frame as in *Figure 1(b)*, in which the FDBS is replaced by a two-diagonal CBS, is obtained by adding the response contributions provided by each of the two diagonal braces and taking into account the load time-history of each of them and the compatibility of the displacements.

Criterion of comparison betwen FDBS and CBS

Assuming the mass distributed along the rigid beam to be the same in both cases, bracing systems having the same average value of stiffness in the elastic phase will be compared. To make the next notations clearer, the subscriptions $(\,)_d$ and $(\,)_c$ will also be adopted for the symbols f_{cr} and f_y when they refer to FDBS and CBS, respectively.

The average value of stiffness for the FDBS, $\tilde{k}_d$, can be defined as the ratio between the horizontal force producing the slippage of both friction joints, given by equation (5), and the corresponding displacement of the rigid beam. Considering equation (3), the latter quantity is expressed by

$$\delta_s = \Delta_1 + \Delta_2 + \Delta_3 = \frac{\cos\alpha}{k_{o,d}}[P_{cr} + (P_l - P_{cr})(l_1 + l_2)] \tag{14}$$

Therefore, considering that $l_1 + l_2 \simeq 2$ one obtains

$$\tilde{k}_d = \frac{F_{u,d}}{\delta_s} = k_{o,d}\frac{2P_l}{2P_l - P_{cr}} = k_{o,d}\frac{2}{2 - \psi_d} \tag{15}$$

where

$$\psi_d = \frac{f_{cr,d}}{f_l} \leq 1 \tag{16}$$

is defined in the same way as in equation (10) for the CBS by replacing the yielding stress $f_{y,c}$ by the stress f_l corresponding to the local slip load.

Considering equation (1), the condition that the slippage of the friction joints occur before the tension braces reach the yielding stress provides

$$f_l \leq \frac{1}{2}(f_{y,d} + f_{cr,d}) \tag{17}$$

Therefore, using equations (16) and (17), the range of design values of ψ_d is defined as

$$\frac{2f_{cr,d}}{f_{y,d} + f_{cr,d}} \leq \psi_d \leq 1 \tag{18}$$

The average value of lateral stiffness for the CBS is given by the ratio between the horizontal force producing the first yielding of the tensile brace and the corresponding horizontal displacement of the rigid beam of the frame. Setting $tg\ \alpha_1 = 0$ in the second branch of the diagram in *Figure*

Table 1

Branch of cycle	Dimensionless stiffness $\tilde{k}_{i,c} = k_{i,c}/k_{o,c}$	Dimensionless inelastic reaction $\tilde{F}_{oi,c} = F_{oi,c}/k_{o,c}$
1	1	0
2	$-\frac{1}{\psi_c}\,\mathrm{tg}\,\alpha_1$	$\delta_y(\psi_c + \mathrm{tg}\,\alpha_1)$
3	0	$\delta_y[\psi_c + (1 - \Delta\bar{\varepsilon}_2)\mathrm{tg}\,\alpha_1]$
4	$\frac{1}{\psi_c}\,\mathrm{tg}\,\alpha_2$	$\delta_y[\psi_c + (1 - \Delta\bar{\varepsilon}_2)\mathrm{tg}\,\alpha_1 - \Delta\bar{\varepsilon}_{r1}\mathrm{tg}\,\alpha_2]$
5	0	$-\delta_y[\psi_c + (1 - \Delta\bar{\varepsilon}_2)\mathrm{tg}\,\alpha_1]$
6	$\frac{1 - \psi_c - (1 - \Delta\bar{\varepsilon}_2)\mathrm{tg}\,\alpha_1}{1 + \psi_c(\Delta\bar{\varepsilon}_5 + c\Delta\bar{\varepsilon}_{r1})}$	$-\delta_y\frac{[\psi_c + (1 - \Delta\bar{\varepsilon}_2)\mathrm{tg}\,\alpha_1](1 + c\psi_c\Delta\bar{\varepsilon}_{r1}) + \psi_c\Delta\bar{\varepsilon}_5}{1 + \psi_c(\Delta\bar{\varepsilon}_5 + c\Delta\bar{\varepsilon}_{r1})}$
7	0	$-\delta_y$
8	1	$-\delta_y(1 - \psi_c\Delta\bar{\varepsilon}_{r2})$

4 (this assumption leads to an acceptable approximation) the former quantity is expressed by

$$F_{u,c} = f_{y,c}\,A_c(1 + \psi_c)\cos\alpha \tag{19}$$

Therefore, considering equations (12) and (13), one obtains

$$\tilde{k}_c = \frac{F_{u,c}}{\delta_y} = k_{o,c}(1 + \psi_c) \tag{20}$$

On the basis of equations (15) and (20) FDBS and CBS can be assumed to be comparable with one another when

$$k_{o,d}\left(\frac{2}{2 - \psi_d}\right) = k_{o,c}(1 + \psi_c) \tag{21}$$

For the intermediate values of ψ_d in the field defined by equation (18), the proposed criterion of equivalence leads to different cross-sectional area values in the two systems.

Parameters governing dynamic responses

The equation of motion of the system in *Figure 1(b)* subjected to ground acceleration, can be written as

$$\ddot{\delta} + 2\omega_d\zeta\dot{\delta} + \omega_d^2(\delta - \delta_o^*) = A_{max}\,\ddot{\bar{s}}_g - \frac{F_{o,d}}{m} \tag{22}$$

where ζ is the damping ratio, $\ddot{\bar{s}}_g(t)$ is the instantaneous ground acceleration normalized with respect to its maximum value A_{max},

$$\omega_d(t) = \left(\frac{k_d(t)}{m}\right)^{1/2} \tag{23}$$

is the instantaneous frequency and $F_{o,d}(t)$ the inelastic reaction, both the latter depending on the branch of the cycle in *Figure 3* involved at the instant of time t.

Assuming equation (17) and consequently equation (18) to be satisfied, i.e. calibrating the slip load to prevent inelastic deformation in the tensile brace, the horizontal branches of the cycle in *Figure 3* are due only to the slippage of the friction device, as specified above. However, a useful comparison between CBS and FDBS can be made by giving the same meaning to these branches as in the CBS cycle, where they correspond to plastic behaviour. On this basis, the instantaneous equivalent ductility demand of the FDBS can be defined as

$$\mu(t) = \frac{\delta(t)}{\delta_s} \tag{24}$$

Therefore, considering equation (24) and defining the strength level factor[15] as

$$\eta = \frac{F_{u,d}}{m\,A_{max}} \tag{25}$$

equation (22) can be rewritten in the form

$$\ddot{\mu} + 2\omega_d\zeta\dot{\mu} + \omega_d^2(\mu - \mu_o^*) = \frac{\tilde{\omega}_d^2}{\eta}\ddot{\bar{s}}_g - \frac{F_{o,d}}{m\delta_s} \tag{26}$$

in which μ_o^* is the residual equivalent ductility value computed in the previous cycles, and

$$\tilde{\omega}_d = \frac{2\pi}{\tilde{T}_d} = \left(\frac{\tilde{k}_d}{m}\right)^{1/2} \tag{27}$$

is the average frequency of the system corresponding to the stiffness expressed by equation (15).

By means of equations (6) and (15), the instantaneous frequency can be related to the average frequency by

$$\omega_d(t) = \tilde{\omega}_d\left(\frac{1 - \frac{\psi_d}{2}}{c_1(t)l_b + c_2(t)l_p}\right)^{1/2} \tag{28}$$

Moreover, equation (9) shows that the ratio $F_{o,d}/(m\delta_s)$ appearing in equation (26) depends on the values of the expression on the right side of equation (28) corresponding to the various branches of the $F - \delta$ cycle in *Figure 3*, and on the ratios between the displacements expressed by equations (3) and δ_s. Therefore, the dynamic response of

the system in *Figure 1(b)* normalized with respect to the value δ_y and corresponding to the input shape contained in $\ddot{\bar{s}}_g(t)$, depends on the following quantities: the average value of the period $\tilde{T}_d$, the factor η, the damping ratio ζ, the stress ratio ψ_d and the geometrical paramters α, l_p and l_b.

The equation of motion of the frame of *Figure 1(b)*, supposed to be braced by a CBS, can be written analogously to equation (26), replacing the subscript $(\ )_d$ by $(\ )_c$, and δ_y by δ_{yc}. The latter substitution, obviously, must first be made in equation (24).

For this system the average frequency can be defined using the stiffness value of equation (20). Moreover, considering the expressions in *Table 1* for a single brace, it can easily be demonstrated that the instantaneous frequency and the ratio $F_{o,c}/(m\delta_y)$ can be related to the average frequency and to the ratio ψ_c. Therefore, the parameters governing the normalized dynamic response of the frame braced by a CBS, for a given shape of input accelerogram, are $\tilde{T}_c$, η, ζ, ψ_c and α. These parameters are quantities analogous to those ruling the FDBS response, except l_b and l_p which are now meaningless. Actually, remembering the comments on the cycle shown in *Figure 4*, in the case of CBS the slenderness and the shape of the cross-section of the braces should be considered as further quantities characterizing the response. Nevertheless, the factor c can be assumed with good approximation to be equal to 0.07 for all the usual sections, as in Maison and Popov[14]; moreover, the values of α_1, α_2 and $\Delta\bar{\varepsilon}_2$ are affected by meaningful variation only if a substantial variation in the slenderness value is considered. Therefore, numerical results can be assumed to correspond to a class of slenderness values, rather than only be valid for a precisely defined slenderness value.

Analysis of dynamic responses

Input characterization

The dynamic responses of the two different bracing systems were evaluated by step-by-step integration of the equation of motion (26) for the FDBF and of the analogous equation for the CBS. The integration step in all the analyses was assumed to be less than 1/50 of the initial period of vibration of the system examined. Five artificial input accelerograms $\ddot{\bar{s}}_g(t)$ with duration $\tau = 25$ s were generated, ensuring their compatibility with the elastic response spectrum of type B proposed in EC8[16], normalized with respect to the maximum acceleration.

This spectrum was amplified considering that the damping ratio for the systems examined was assumed to be $\zeta = 0.01$. Consequently, its maximum ordinate was deduced from the expression

$$\beta_o = 2.5\left(\frac{0.05}{\zeta}\right)^{1/2} = 5.59$$

which is provided by EC8 itself.

Each of the input accelerograms is a stationary process[17], modelled during the first $0.1\,\tau$ s by the envelope function

$$\xi(t) = 0.5\left(1 - \cos\frac{\pi t}{0.1\,\tau}\right)$$

as done by Preumont[18] to minimize the effect of the transient phase of the response.

Figure 5 shows the normalized elastic response spectrum obtained by the average values of the response spectra corresponding to the single accelerograms utilized, and that deduced by EC8 as specified above. The range of periods considered includes the values which can realistically be expected for structural systems as in *Figure 1(b)*. The results will be presented later as average values of those which were deduced from the five input accelerograms utilized.

Structural parameters of systems examined

The following values of geometrical parameters were assumed for the systems examined: $\alpha = 30°$ for both types of bracing systems; $l_p = 0.1$ and $l_b = 0.45$ for the FBDS. The latter are very common values for the sizes of friction damping devices.

For the FBDS the parameter ψ_d was assumed to have the minimum value in the range of equation (18). Setting this value $\psi_d = 0.43$ and the slenderness of the diagonal braces $\lambda = 150$, the yielding stress proves to be $f_{y,d} = 320$ N/mm^2. Adopting the same values of slenderness and yielding stress, the value $\psi_c = 0.27$ was deduced for the CBS.

On the basis of these assumptions, the global slip stress on the tension braces of the FDBS, $f_s = 2f_l - f_{cr,d}$, is equal to the yielding stress at which the plastic behaviour of the tension braces of the CBS occurs. However, this circumstance does not imply loss of generality in the conclusions which will be deduced, as will be clearly shown later.

Ductility demand

Figures 6(a) and *6(b)* show the maximum ductility demand versus average period curves for the FDBS (equivalent ductility) and the CBS, with variation in the factor η. For simplicity's sake, in both figures the average periods $\tilde{T}_d$ and $\tilde{T}_c$ are indicated by the same symbol T.

For low values of η the curves concerning the FDBS exhibit a marked irregularity due to the highly scattered results provided by the single responses to the accelerograms utilized. This phenomenon, which was already observed by Mezzi *et al.*[19], can be justified by considering the stable shape of the cycle in *Figure 3*. A friction damped braced frame usually undergoes one noticeable translation when an input acceleration peak occurs. The subsequent oscillations happen with respect to the new position and

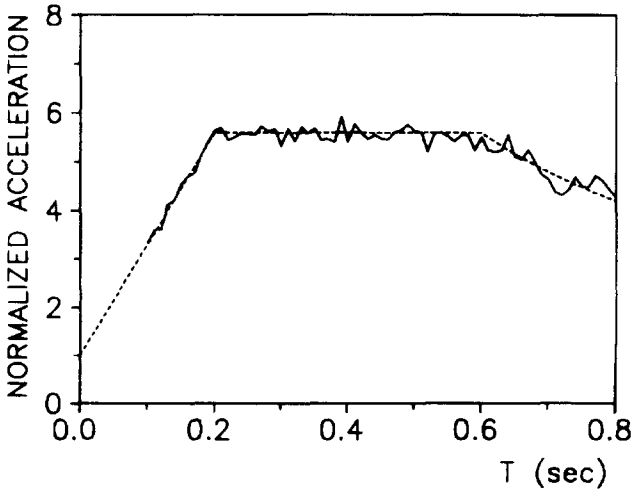

Figure 5 Average response spectrum of input accelerograms used (——), and response spectrum proposed by EC8 (– – –) for $\zeta = 0.01$

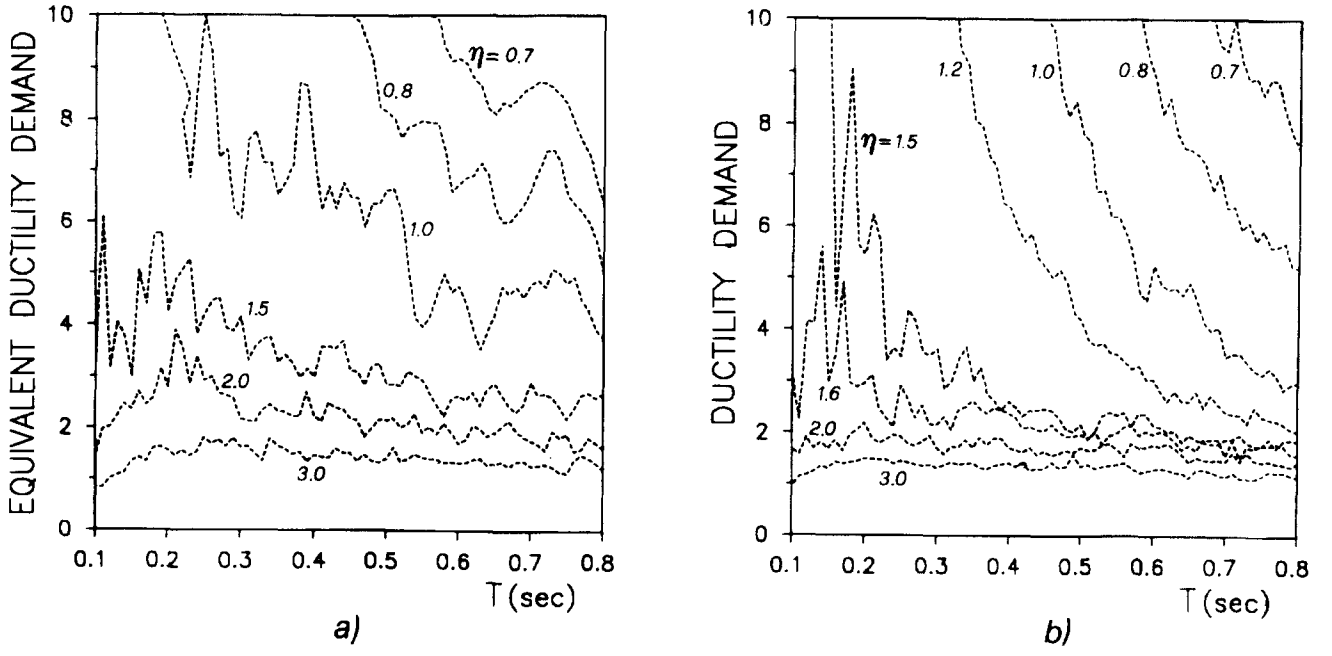

Figure 6 Ductility demand with variation in strength level factor. (a) FDBS (equivalent ductility); (b) CBS

further translations are very small because the buckled braces of the system almost instantaneously recover the straightened configuration and, consequently, their stiffness. As the occurrence of a peak input acceleration and its recurrence during the same input are random events, scattered maximum values of displacement can be obtained under different ground motion time-histories. The consideration above is confirmed by the fact that the equivalent ductility demand curves tend to assume a regular shape when the factor η increases, i.e. when the global slip load of the device is adjusted to a higher value.

The greater regularity of the curves in *Figure 6(b)* for the CBS, even for low values of η, is due to the progressive translation of the hysteresis cycles of the single diagonal brace, which is produced by the irreversibility of the tensile plastic deformations. Whenever the frame motion is reversed, the CBS meaningfully recovers its effectiveness only after the maximum displacement of the previous cycle is exceeded. Therefore, in the presence of high-intensity ground accelerograms the amplitude of the oscillations of the system increases progressively and the maximum response value is only slightly influenced by the input random nature.

The curves in *Figures 7(a)* and *7(b)* were derived from those in *Figures 6(a)* and *6(b)*, respectively, by manipulation of the numerical results based on the least squares method. Moreover, a higher number of values of the strength level factor in the range $0.7 \leq \eta \leq 3.5$ was considered. The comments on the results in the figures will be made, for simplicity's sake, assuming the systems to have fixed mechanical and geometrical characteristics and the variation in the factor η to be due to a variation in the value of the maximum input acceleration A_{max}.

For small values of the input intensity (high values of η) the equivalent ductility demand in the FDBS and the actual ductility demand in the CBS are almost independent of the average period of vibration and they remain lower than 2 for $\eta \geq 2.5$ in the FDBS and for $\eta \geq 2$ in the CBS. When A_{max} increases, the performance of the two systems tend to differ from one another, especially in the range of low periods (highly stiff systems). In the range $0.1 \text{ s} \leq T \leq 0.35$ s, as long as the strength level factor remains $\eta \geq 1.6$ the CBS proves to be more effective than the FDBS, since it requires a lower ductility value, which in all cases is $\mu \leq 4$. By contrast, for $\eta < 1.3$, the CBS proves to be absolutely inadequate to bear the seismic action, because the ductility demand is certainly higher than that which can realistically be provided by the system. In this field the FDBS is still subjected to an acceptable equivalent ductility demand although the latter, obviously, increases progressively when η decreases. When deformable structures are considered, i.e. for higher values of period, the responses of the two different systems again become comparable with one another.

As already mentioned, the results above are almost independent of the parameter ψ_d. The diagrams in *Figures 8(a)* and *8(b)* show the equivalent ductility demand versus average period curves for FDBS characterized by the same values of the other parameters as in the previous case, but for $\psi_d = 0.6$ and $\psi_d = 0.9$, respectively. In both figures the dotted curves are those already presented in *Figure 6(a)* for the values of the factor η considered. The results show that, when the factor η is assigned, the slip load can be adjusted by using the value of ψ_d, in the range of equation (18) providing the optimum device performance. In all cases the maximum dimensionless response is expressed with very good approximation by the curves in *Figure 7(a)*.

Behaviour factor

Denoting as $R(T)$ the ordinate of the normalized elastic spectrum which was assumed to calibrate the input accelerograms (see *Figure 5*), the behaviour factor is defined as

$$q = \frac{m A_{max} R(T)}{F_u} = \frac{R(T)}{\eta} \tag{29}$$

Therefore, the curves $q(T, \mu)$ can be obtained from those in *Figures 7(a)* and *7(b)* for the two bracing systems by deducing the values of T and η corresponding to each assigned value of μ, and by introducing in equation (29) the corresponding value of $R(T)$ provided by the nor-

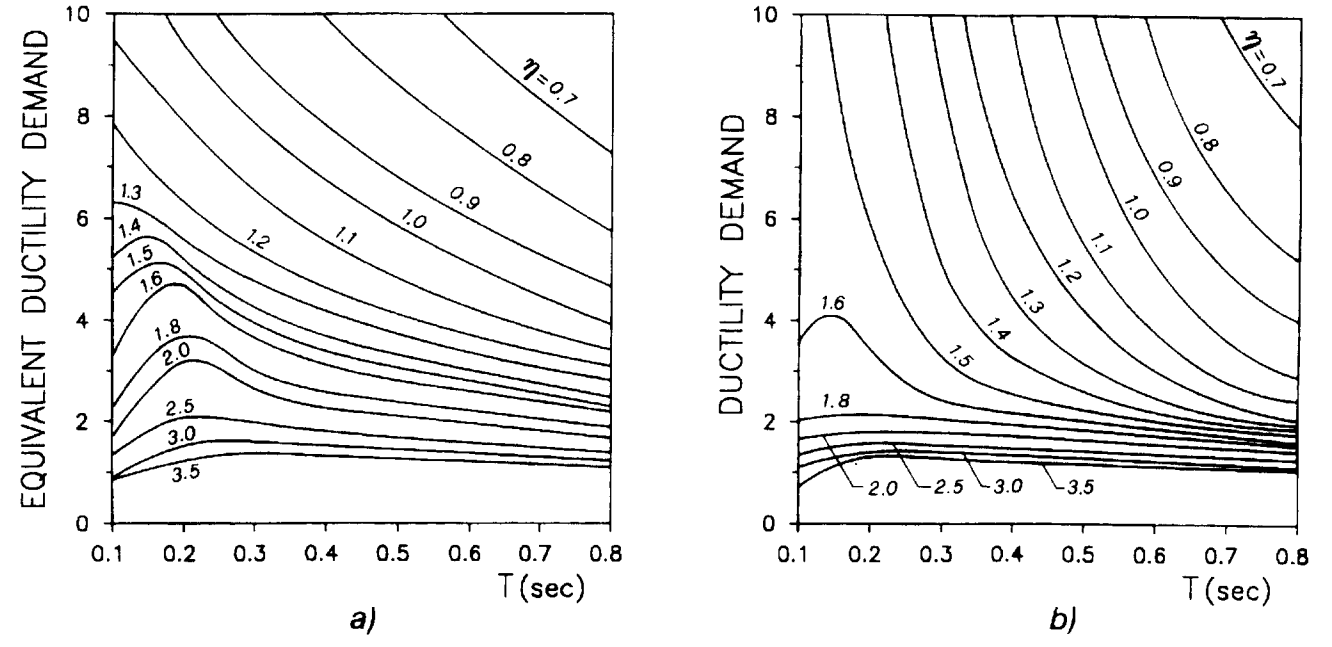

Figure 7 Curves derived by interpolation of results in *Figure 6*. (a) FDBS; (b) CBS

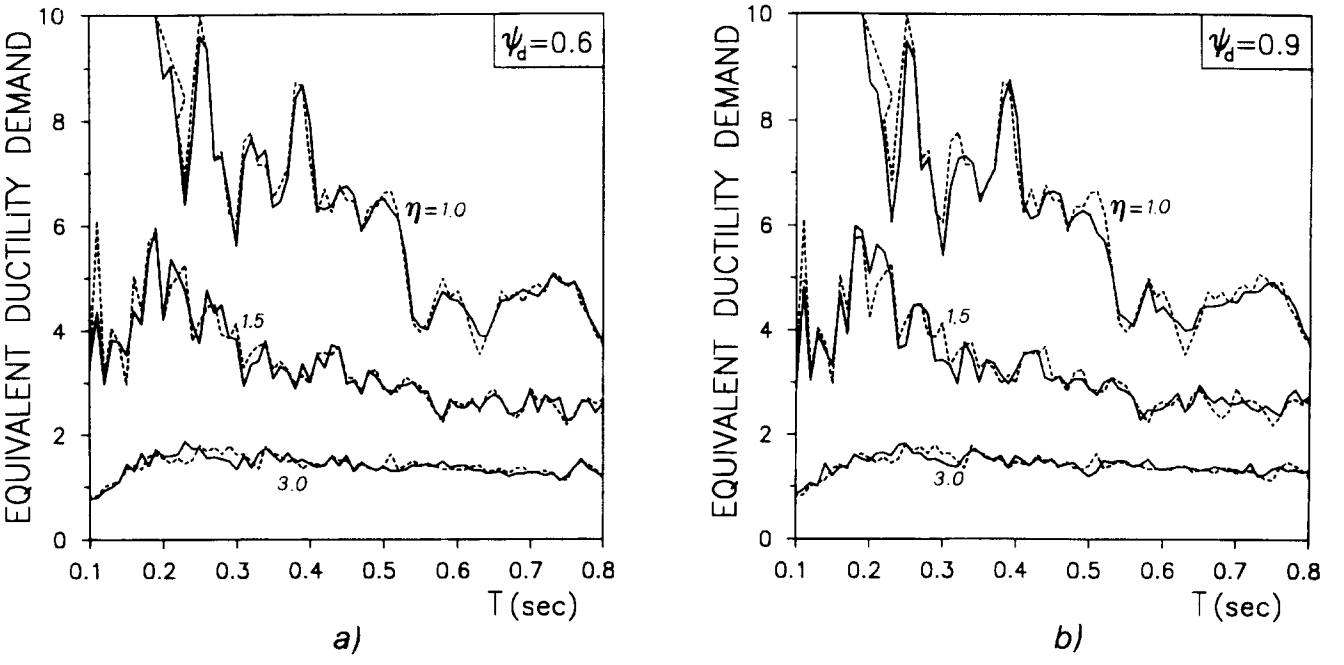

Figure 8 Influence of parameter ψ_d on equivalent ductility demand of FDBS; (– – –) curves for ψ_d = 0.43 as in *Figure 6(a)*

malized spectrum. This procedure leads to the results shown in *Figures 9(a) 9(b)* and for the FDBS and the CBS, respectively.

It should be noted that the curves take into account that whenever $q \geq \mu$ the postelastic resources of the CBS or the slippage capabilities of the FDBS are fully utilizable for economical design, while, when $q < \mu$, the available actual or equivalent ductility does not imply the same level of reduction of design seismic forces and the structural design needs special care. *Figure 9(a)* shows that in the FDBS for values of available equivalent ductility $\mu \leq 2$ the behaviour factor depends little on the average period of the system and proves to be $q > \mu$. When μ increases, the range of period in which the latter condition remains satisfied is reduced, shifting towards higher values (more deformable structures) so that for $\mu = 6$ the relationship $q > \mu$ is not verified for any value of the period. However, adjusting the slip load of the device to obtain higher values of μ, higher values of q can be reached, even if the increases in the behaviour factor prove to be less than the increases in the equivalent ductility demand. In all cases, as expected, the most unfavourable conditions pertain to stiff structures. Assuming the reference value T_o = 0.2 s, as in EC8[16], the curves in *Figure 9(a)* show that for $\mu = 6$ and $T > T_o$ values of the behaviour factor in the range $4 \leq q \leq 6$ can be adopted; if the device allows an available equivalent ductility $\mu = 8$, for $T > T_o$ one obtains $5 \leq q \leq 7$. Considering values of T decreasing from T_o to zero, the behaviour factor can be assumed to be linearly decreasing from the minimum values corresponding to the two cases mentioned above to unity.

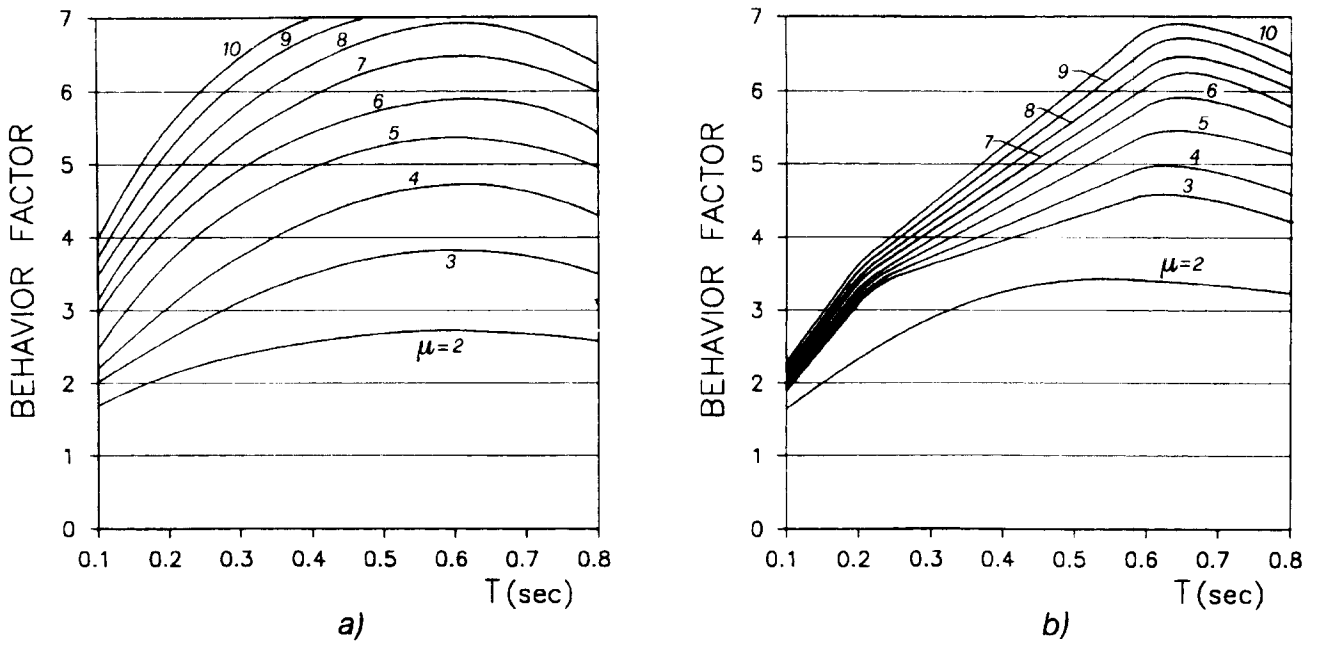

Figure 9 Behaviour factor with variation in available ductility. (a) FDBS; (b) CBS

The diagram in *Figure 9(b)* for the CBS shows that even if an available ductility value $\mu > 3$ is assumed (the values which can realistically be expected for the ordinary cross-bracing system are noticeably lower than the equivalent values referring to the FDBS) the risk condition of the structure is unacceptable, because beyond this value of ductility the curves are extremely close, particularly in the range of low periods. Considering for example a structure having $T = T_0 = 0.2$ s, a variation in the behaviour factor from 3 to 3.5 implies an increase in the ductility demand from 3 to 8, the latter being an unrealistic value to be provided by the system. Therefore, the curve corresponding to $\mu = 3$ must be considered a limit curve and the conservative value of $q = 3$ for $T > T_0$ could be assumed. As for the FDBS, for T decreasing from 0.2 s to zero, the behaviour factor can be assumed linearly decreasing to unity.

For practical use of the results which were derived, the numerical values presented here have to be considered to underestimate the performances of the two systems. This is because they were deduced by means of input accelerograms calibrated on the normalized elastic spectrum in EC8 amplified because $\zeta = 0.01$. This approach, which is conceptually rigorous in deducing the actual values of the behaviour factor, overestimates the input intensity with respect to an analysis based on accelerograms deduced from the standard spectrum (for $\zeta = 0.05$) as EC8 itself prescribes. Moreover, specially for the CBS, the stationary nature[17] of the artificial accelerograms implies higher values of ductility demand than those corresponding to more realistic nonstationary input simulations.

Application examples

The system in *Figure 1(b)* and that obtained replacing the FDBS with an equivalent CBS were considered to be subjected to the first 25 s of the SOOE component of the Imperial Valley (El Centro, 1940) earthquake. The following specifications were assumed for both systems; m = 15 000 Kg; $\zeta = 0.01$; H = 300 cm = height of storey; D = 520 cm = span length. Therefore, the values L = 600 cm and $\alpha = 30°$ were deduced.

The diagonal braces of the FDBS were assumed to be angles of section $4 \times 4 \times 1/4$, to which the values A_d = 1251 mm^2, λ = 149 (slenderness), $f_{cr,d}$ = 89 N/mm^2 correspond. Assuming $f_{y,d}$ = 320 N/mm^2 and the minimum value of ψ_d in equation (18), equation (16) provides f_l = 204 N/mm^2. The device geometry was defined assuming the value L_p = 60 cm, which, considering the value of length L, leads to L_b = 270 cm. Moreoever, equations (14), (5), (15) and (27) provide the quantities δ_s = 1.108 cm, $F_{u,d}$ = 442 KN, $\tilde{T}_d$ = 0.39 s. Assuming the same yielding stress and considering the value of ψ_d, the data specified for the FDBS remain valid for the CBS, for which one also obtains $\delta_y = \delta_s$ and $F_{u,c} = F_{u,d} = F_u$.

In order to point out the different behaviours of the two bracing systems with variation in the input intensity, the input accelerogram in a first case was considered to be affected by its actual maximum value $A_{max,1} = 0.35\ g$, where g is the acceleration due to gravity; in a second case it was scaled to a maximum value $A_{max,2} = 0.5\ g$. The corresponding strength level factor values for both systems are η_1 = 0.875 and $\eta_2 = 0.612$, respectively. The structural responses of the two systems can be predicted by the curves in *Figure 7*, scaling by a suitable factor χ the normalized elastic response spectrum of the accelerogram considered to make it as close as possible to the EC8 spectrum.

This procedure leads to the value $\chi = 1.6$. Therefore, the curves in *Figure 7* can provide good approximate values of the dimensionless responses in the two cases, by amplifying the values of the actual factor η by χ, which leads to $\eta_1^* = 1.4$ and $\eta_2^* = 1.00$.

With reference to the first value and for $T = 0.39$ s, *Figures 7(a)* and *7(b)* provide $\mu = 3.74$ for the FDBS and $\mu = 3.40$ for the CBS, respectively. *Figures 10(a)* and *10(b)* show the time-histories of the responses of the two systems deduced by means of the step-by-step integrations of the equations of motion. At the instant of time $t = 5.11$ s the friction damped braced frame reaches the maximum dis-

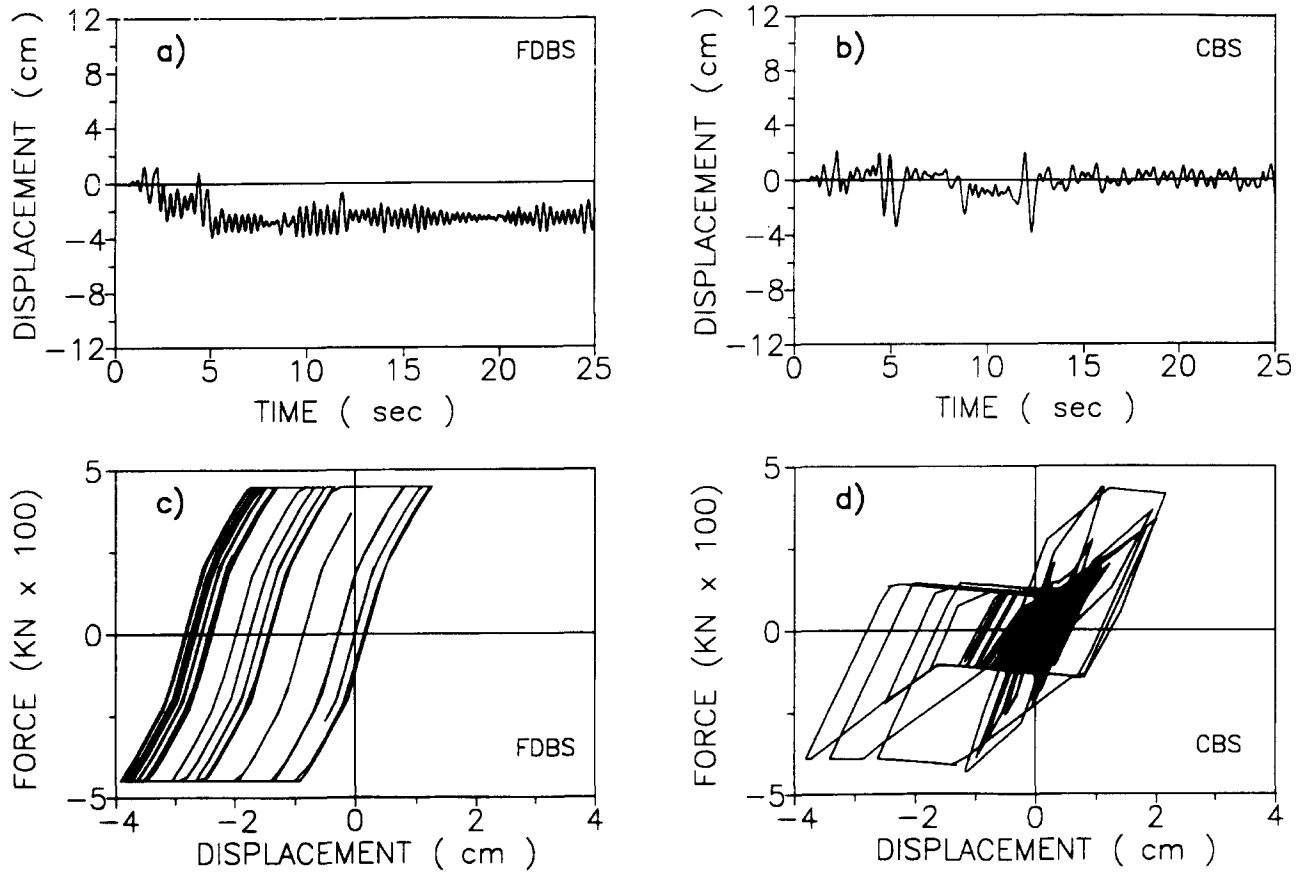

Figure 10 Dynamic responses for $A_{max} = 0.35\ g$. (a) and (b) time-histories of lateral displacement; (c) and (d) $F - \delta$ cycles

placement of 3.91 cm, corresponding to an equivalent ductility demand of 3.53, very close to the predicted value. During the following time the system undergoes oscillations of moderate amplitude around a position different from the initial one. This phenomenon could be reduced by using the FDBS in parallel with back-up frames with minimal moment resisting capabilities, providing an elastic restoring effect.

The maximum displacement of the frame braced by the CBS proves to be 3.80 cm, corresponding to a ductility demand value of 3.43, almost coincident with the expected one. This value is reached after 12.4 s. The presence of large amplitude oscillations even when $t > 6$ s and the input has already exhausted its highest peaks of acceleration, reveals the loss of stiffness of the system due to the delay of each diagonal brace in recovering the straightened configuration after buckling.

Figures 10(c) and *10(d)* show the cycles $F - \delta$ for the two different braced frames. A detailed analysis of the results showed that the first five cycles, occurring in the range of time $0 \leq t < 5.93$ s, are qualitatively very similar for the two systems and the amount of dissipated energy can also be evaluated to be of the same order. In the subsequent cycles the FBDS is able to dissipate energy by small slippage of the device as in the initial phase of the motion, while the CBS needs displacements of increasing amplitude to absorb further amounts of energy, because of the loss of initial stiffness due to the noticeable plastic tensile deformations produced by the previous acceleration peaks.

These comments make it possible to foresee the absolutely different responses of the two systems in the case in which the maximum peak of the input acceleration is assumed to be $A_{max,2} = 0.5\ g$. *Figure 7* for $\eta_2^* = 1.00$ and $T = 0.39$ s provides $\mu = 6.84$ and $\mu > 10$ for the FDBS and the CBS, respectively. The time-histories of the responses obtained by the step-by-step procedure are shown in *Figures 11(a)* and *11(b)*. The maximum horizontal displacements prove to be 7.42 cm ($\mu = 6.70$) and 10.55 cm ($\mu = 9.52$) for the FDBS and the CBS, respectively. The FDBS undergoes large displacements only in the range of time during which the input excitation reaches its greatest values; later, the stability of the hysteresis cycles implies oscillations of moderate amplitude. By contrast, the maximum displacement reached influences the response of the CBS for all the duration of the seismic excitation.

Figures 11(c) and *11(d)* show the cycles $F - \delta$ for the two systems, confirming the comments above. Finally, it must be observed that the response of the CBS was evaluated neglecting possible brittle behaviour due to fatigue phenomena and effects of concentration of plastic deformations in critical regions, which often produce bracing failure.

Conclusions

The reliability level of friction damped braced systems and of ordinary cross-bracing systems having slender braces was investigated by step-by-step analyses of their seismic responses.

The comparison between the different performances was carried out by first deriving a relationship between the structural parameters characterizing the two kinds of brac-

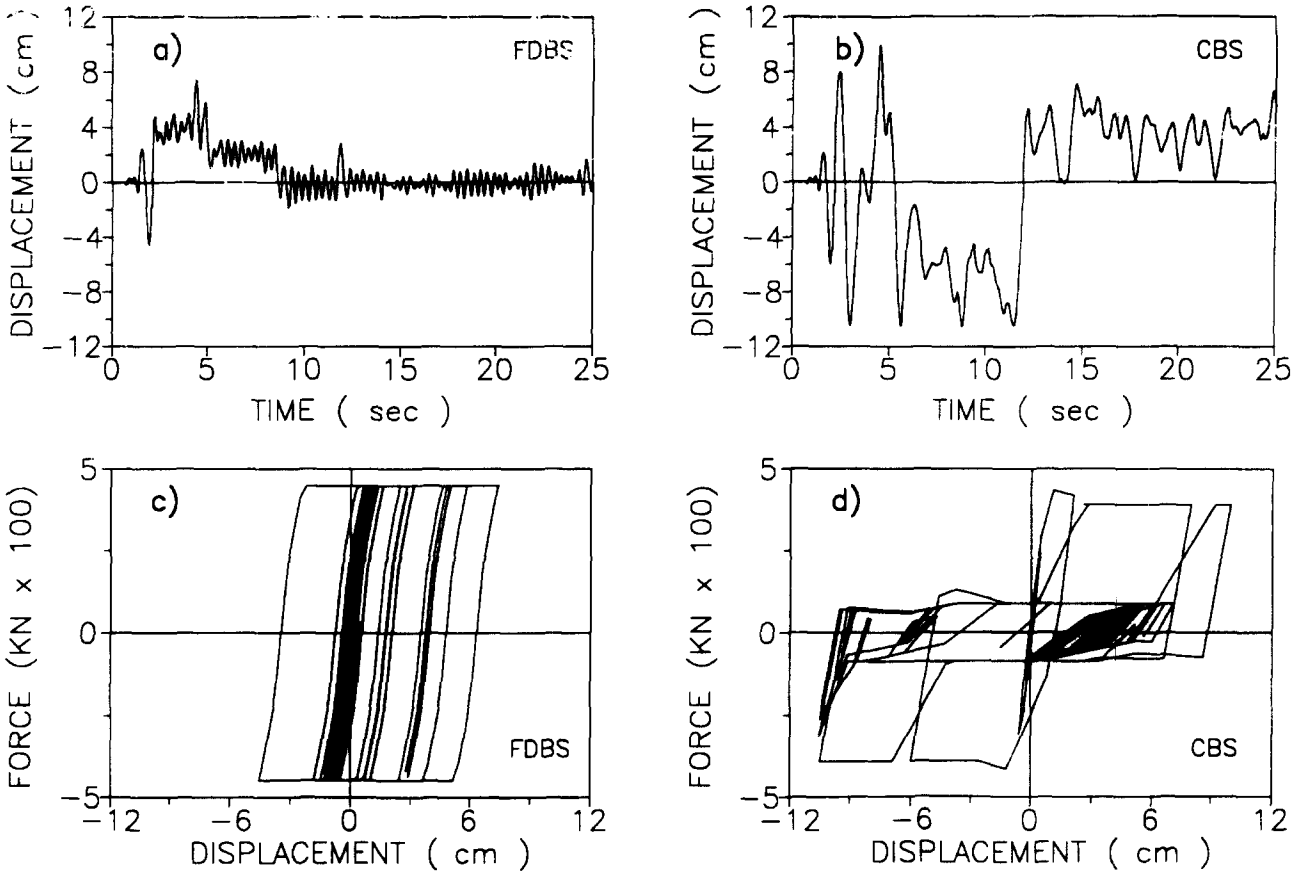

Figure 11 Dynamic responses for A_{max} = 0.5 *g*. (a) and (b) time-histories of lateral displacement; (c) and (d) $F - \delta$ cycles

ing system, leading to the same value of the average period of vibration.

The results show that the assumption of an available ductility value greater than 3 for the CBS implies a high risk condition, apart from fatigue and localized plasticity effects. Designing cross-braced structures for a behaviour factor slightly higher than that corresponding to the ductility value above, the ductility demand increases abruptly between two and three times, particularly in the range of low periods, which implies an unacceptable damage level in the structure and likely failure of the diagonal braces.

Otherwise, adjusting the slip load of the FDBS to a suitable value, higher values of behaviour factor can be used for design purposes, without the risk of a wrong estimate of the input intensity endangering system safety.

The different level of seismic protection of the two systems depends on the way the force–displacement hysteresis cycles go, which can be summarized as follows. The FDBS relates its instantaneous seismic response to the current excitation intensity, because of the stability of the $F - \delta$ cycles; in the CBS the irreversible loss of stiffness due to the large plastic deformations produced by peaks of the input acceleration, influences the response during the whole earthquake.

References

1 Pall, A. S. and Marsh, C. 'Response of friction damped braced frames', *J. Struct. Div., ASCE* 1982, **108**(ST6), 1313–1322

2 Filiatrault, A. and Cherry, S. 'Performance evaluation of friction damped braced steel frames under simulated earthquake loads', *Earthquake Spectra* 1987, **3**(1), 57–87

3 Filiatrault, A. and Cherry, S. 'Comparative performance of friction damped systems and base isolation system for earthquake retrofit and aseismic design', *Earthquake Engng Struct. Dyn.* 1988, **16**(3), 389–416

4 Filiatrault, A. and Cherry, S. 'Seismic design of friction damped braced steel plane frames by energy methods', Earthquake Engineering Research Laboratory Report UCB-EERL-88-01, Department of Civil Engineering, University of British Columbia, Vancouver, Canada, 1988

5 Filiatrault, A. and Cherry, S. 'Efficient numerical modelling for seismic design of friction damped braced steel plane frames', *Can. J. Civ. Engng* 1989, **16**(3), 211–218

6 Giacchetti, R., Whittaker, A. S., Bertero, V. V. and Aktan, H. M. 'Seismic response of a DMRSF retrofitted with friction slip devices', *Proc. Int. Meeting on Base Isolation and Passive Energy Dissipation*, Assisi, Italy, 1989

7 Whittaker, A. S., Bertero, V. V., Alonso, J. and Thompson, C. 'Earthquake simulator testing of steel plate added damping and stiffness elements', Report UCB/EERC-89-02, Earthquake Engineering Research Center, University of California, Berkeley, January, 1989

8 Ciampi, V. and Samuelli Ferretti, A. 'Energy dissipation in buildings using special bracing systems', *Proc. 9th European Conf. Earthquake Engng*, Moscow, 1990

9 Filiatrault, A. and Cherry, S. 'Seismic design spectra for friction damped structures', *J. Struct. Div., ASCE* 1990, **116**(ST5), 1334–1355

10 Ciampi, V., Arcangeli, M. and Ferlito, R. 'Dissipative bracings for seismic protection of buildings', *Proc. Int. Meeting on Earthquake Protection of Buildings*, Ancone, Italy, 1991

11 Vulcano, A. 'Nonlinear seismic response of damped braced frames', *Proc. Int. Meeting on Earthquake Protection of Buildings*, Ancone, Italy, 1991

12 Ballio, G. and Campanini, G. 'Comportamento di aste di controvento soggette a cicli alterni di carico', *C.T.A.*, Palermo, Italy, October 1981 (in Italian)

13 Popov, E. P., Takanashi, K. and Roeder, C. W. 'Structural steel bracing systems: behaviour under cyclic loading', Report UCB/EERC-76/17 Earthquake Engineering Research Center, University of California, Berkeley, June 1976

14 Maison, B. and Popov, E. 'Cyclic response prediction for braced steel

frames', *J. Struct. Div., ASCE* 1980, **106**(ST7), 1401–1416
15 Mahin, S. and Bertero, V. V. 'An evaluation of inelastic seismic design spectra', *J Struct. Div., ASCE* 1981, **107**(ST9), 1777–1794
16 Commission of European Communities, *Eurocode 8. Structures in seismic regions*, Brussels, Belgium, 1988
17 Clough, R. W. and Penzien, J. *Dynamics of structures*, McGraw-Hill Kogakusha, 1975
18 Preumont, A. 'The generation of spectrum compatible accelerograms for the design of nuclear plants', *Earthquake Engng Struct. Dyn.* 1984, **12**(4), 481–497
19 Mezzi, M., Radicchia, R. and D'Ambrisi, A. 'Use of artificially generated accelerograms in the seismic analyses of nonlinear structures', *Proc. Int. Meeting on Earthquake Protection of Buildings*, Ancone, Italy, 1991